

# Optimizing and comparing the design of a cathode catalyst layer by providing electron continuous paths for improving the performance of proton exchange membrane fuel cells

Chih-Jui Lung<sup>a,\*</sup>, Hsiu-Li Lin<sup>a,b</sup>

<sup>a</sup>Department of Chemical Engineering & Materials Science, Yuan Ze University, Chung-Li, Taoyuan 32003, Taiwan

<sup>b</sup>Fuel Cell Center, Yuan Ze University, Chung-Li, Taoyuan 32003, Taiwan

## HIGHLIGHTS

- Carbon fibers (CFs), multi-walled carbon nanotubes (MWCNTs), and vapor-grown carbon fibers (VGCFs) were simply and directly added to cathode catalyst layers.
- CFs, MWCNTs, and VGCFs improved the performance of proton exchange membrane fuel cells by 96%, 73%, and 54%, respectively.
- The concept of electronic conducting continuity is introduced by investigating the improvement in performance after the addition of CFs, MWCNTs, and VGCFs.

## ARTICLE INFO

Keywords:

Proton exchange membrane fuel cells

Carbon fibers

Multi-walled carbon nanotubes

Vapor-grown carbon fibers

Cathode catalyst layer

## Abstract

Herein, the performance of proton exchange membrane fuel cells (PEMFCs) is improved by modifying cathode catalyst layers (CCLs) through the direct addition of multi-walled carbon nanotubes (MWCNTs), vapor-grown carbon fibers (VGCFs), and carbon fibers (CFs). The optimal weight percentage (wt) of these three carbon materials is approximately 6 wt% after measuring the pristine (0 wt%), 1 wt%, 3 wt%, and 6 wt% contents of theirs. Among the additives, the addition of CFs results in the highest improvement in the performance. When the temperature is maintained at 80 °C, the anode side and cathode side have a relative humidity (RH) of 100%, stoichiometry of reactant is 1.5 and 2.0, and in the absence of backpressure, the highest power density reaches 450 mWcm<sup>-2</sup>, which increases by 96% than that of the pristine. The MWCNTs and VGCFs increase the power density of PEMFCs by 73% and 54%, respectively.

---

\* Corresponding author.

E-mail address: [daniel31108128@gmail.com](mailto:daniel31108128@gmail.com) (C.-J. Lung)

## 1. Introduction

Environmental pollution caused by fossil fuel has been considered as one of the most severe global problems and has been proactively discussed among several nations in recent decades. With high energy conversion efficiencies, safe operation, and insignificant pollutant byproducts, proton exchange membrane fuel cells (PEMFCs) have emerged as promising power sources that can be applied in vehicles and portable electronic equipments [1]. Currently, Pt is the most effective catalyst in use, and thus, Pt nanoparticles supported on carbon blacks (CBs) are generally employed as composite electrocatalysts to accelerate electrochemical reactions for both anodes and cathodes [2]. Although composite catalysts are able to reduce the amount of Pt loading with slight performance sacrifices, the most significant barrier that PEMFCs face toward commercial market penetration remains their high cost. Moreover, Pt particles are not fully utilized in the catalyst layer because they are easily covered by most CBs [3]. Therefore, a triple phase boundary (TPB) is introduced, wherein the surface area of the catalyst is in contact with the electrolyte, gas, and electronic materials conductor [4,5]. Recently, the demand for automotive applications has boosted the fuel cell chains and introduced challenging performance and cost aspects required for PEMFCs.

Membrane electrode assembly (MEA), which is one of the core factors influencing the performance of PEMFCs, can obtain high performance by designing an active electrode to increase the amount of TPB [6,7]. In light of the close contact of the catalyst layers with the gas diffusion layer (GDL) and the membrane contributing to high performance, fast electron and proton transport is required, and some suitable voids are required to allow the reactant and product to flow. Although the carbon support type, Pt catalyst loading in the catalyst layer, and Nafion® content, which are the three main parameters affecting performance, were identified by Weber [8], there is still a need to explore an easier and more feasible way to increase performance. The design of CCLs is more appealing to researchers than that of anodes because of the more sluggish electrocatalytic activity of oxygen reduction and the more sophisticated liquid-gas transfer process involved [9-11]. Consequently, apart from designing the microscopic structure of the catalyst layers, factors including the ionomer content, electron contacts, layer porosity, and pressing conditions are all interrelated and should be meticulously considered in order to create an optimal electrode design [12,13].

The majority of researchers have indicated that alloying Pt with transition metals is a beneficial method that can increase electrocatalytic activity and durability [14-16]. Although this effect can improve the performance and effectively reduce the cost of Pt, the synthesis processes are troublesome and unstable because they require complicated steps, such as reduction reactions. In addition, various carbon materials are utilized to increase the performance of Pt growth to obtain better electrocatalytic activity and dispersion [17,18]. CNTs have been widely considered for various types of fuel cells as materials with outstanding electrical and heat conductivities [19]. Hou *et al.* [20] found that an MWCNT-doped microporous layer (MPL), which can provide a porous structure, wettability, and electronic conductivity to facilitate reactant and water transport between the catalyst layers and flow field plate, showed better performance than an MPL with CBs. This result was attributed to the presence of advanced transport properties, including enhanced reactant transportation and water

management, as well as reduced electronic resistance. As a catalyst support, Haque *et al.* [21] observed that Pt/MWCNT catalysts can enhance Pt activity by increasing porosity, and thus, they can achieve excellent PEMFC performance. Moreover, Kaneko S. *et al.* [22,23] found that the superior corrosion resistance resulted from CNTs compared with using common catalyst supports based on CBs. However, there are some disadvantages associated with fabricating carbon materials as Pt supports. First, high-temperature environment is required for preparing the carbon materials if chemical vapor deposition (CVD) is used for gasification [24]. Treatments may be difficult and unstable and may result in unnecessary power consumption [25,26]. Second, oxidation–reduction and hydrogenation consisting of sophisticated procedures are highly likely to result in low preparation reproducibility because inconsistent amounts of carbon are produced from different batches of identical materials [27,28]. In addition, the high microporosity of activated carbon results in problems with respect to accessibility between the reactants and active sites. D.-H. Jung *et al.* [29] found that the performance of direct methanol fuel cells (DMFCs) can be improved by directly adding small amounts of VGCFs in the preparation of the catalyst ink and placing them in the anode electrode to effectively increase porosity and electron conduction. With high electrical conductivity and nanoscopic dimensions, CNTs can also provide such advantages by directly adding them into the ink to change the microscopic structure of CCLs. Peethambharan *et al.* [30] found that using MWCNT ink enhanced the energy efficiency of flexible heating applications. The procedure for modifying CCLs seems to be complex, regardless of the methods used to enhance the performance. Therefore, directly adding carbon materials to CCLs is a simpler process than the reduction methods.

CFs, CNTs, and VGCFs were selected as additives for the CCLs of PEMFCs in the current study. These materials are non-catalytic components, but they are expected to provide electron paths and effective voids. The fabrication of CCLs by adding CFs has not yet been explored, and the effects of CNTs and VGCFs in CCLs on the performance of PEMFCs need to be further investigated. However, the excessive loading of additives would cause a detrimental effect based on the increase in the thickness of the catalyst layers and the active surface of the compressed Pt [31]. Two main subjects will be presented to investigate the effectiveness and contribution of CFs, CNTs, and VGCFs through a series of examinations. One is to determine the most prominent factor for improving the performance and to find the optimal addition ratio to the catalyst, whereas the other is to rank them in terms of performance by comparing their optimal performance.

## 2. Experimental

### 2.1. Chemicals

A commercial Nafion®-212 membrane was purchased from DuPont Co., and 40 wt% Pt catalyst on carbon black was purchased from Alfa Aesar. SIGRACET 10BC carbon papers as GDLs were purchased from SGL GROUP. Methyl ethyl ketone ( $\text{CH}_3\text{COCH}_2\text{CH}_3$ , MEK) was purchased from Avantor Performance Materials Inc. Potassium chloride (KCl) was purchased from Mallinckrodt AR®. 2-propanol ( $\text{C}_3\text{H}_9\text{OH}$ ) and ethanol ( $\text{C}_2\text{H}_5\text{OH}$ ) were purchased from Sigma-Aldrich Co. LLC. A Nafion® solution (perfluorosulfonic acid resin, 5–6 wt%) was purchased from DuPont Co. containing water (40–50 wt%), propanol (42–54 wt%), ethyl alcohol

(< 8 wt%), mixed ethers, and other VOCs (< 2 wt%). Carbon fibers, C tube-010H MWCNTs, and VGCFs (3  $\mu\text{m}$ ) were purchased from Formosa Taffeta Co., Ltd., Golden Innovation Business Co., Ltd., and UNITETEK International Co. Ltd., respectively. The fundamental properties of these carbon materials are shown in [Table 1](#).

**Table 1** Summary of fundamental properties for carbon materials

Additives	Diameter (nm)	Length ( $\mu\text{m}$ )	Density ( $\text{gcm}^{-3}$ )
CFs	5000–10000	> 50000	1.75–1.93
CNTs (MWCNTs)	5–20	1–2	1.30–1.40
VGCFs	100–500	2–5	1.80–2.00

## 2.2. Fabrication of electrodes

The catalyst-coated membrane (CCM) method was used to manufacture Nafion®-based CCLs with three distinct quantities of CFs, CNTs, and VGCFs with 1, 3, and 6 wt% with respect to the catalyst. The anode side of the catalyst layer was Nafion®-based; its ink principally contained Pt/C and Nafion®. Among the three carbon materials, CFs were manually deposited upon the CCLs because they were too bulky to be added to the ink. The Nafion® membrane needed to be sprayed with ink before fixing the CFs on it, placing the CFs in the middle of the catalyst layer, neither close to the membrane nor to the GDL. A schematic of the fabrication process of adding CFs to the CCLs is shown in [Fig. 1](#). The CNTs and VGCFs could be added to the ink and were sprayed out from a nozzle; thus, weight percentage calculations were exploited to obtain their actual weight before preparing the ink. A Nafion®-based electrode was also prepared by the CCM method, and it was regarded as a pristine for comparison with the above improved CLs. Both the pristine and improved electrodes were based on the Pt/C electrode, which included Pt and Nafion®. The Pt loading was 0.2 and 0.4  $\text{mgcm}^{-2}$  on the anode and cathode side, respectively, and the Nafion® loading was 0.75  $\text{mgcm}^{-2}$ .

A single PEM fuel cell with an active surface area of 2.5 cm  $\times$  2.5 cm was used for all the experiments in this study. The components of the PEM fuel cell (MEA, GDL, bipolar plates, current collectors, gasket, and end plates) were assembled using a method that diagonally exerted a clamping torque of 5 N·m each time to reach 25 N·m.

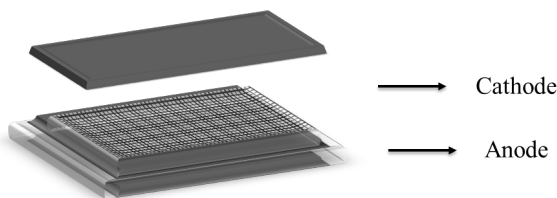


**Fig. 1** Fabrication process of CFs added into the CCLs of MEA

## 2.3. Physical characterization

Scanning electron microscopy (SEM) images were obtained using a JEOL JSM-6701F scanning electron microscope. Furthermore, the values of the electronic resistance of the CCLs with CFs, CCLs with CNTs, and CCLs with VGCFs were acquired using a four-point probing measurement system (KeithLink Technology Co., Ltd.).

## 2.4. Electrochemical characterization

To investigate the performance of the MEAs, a PEM fuel cell was tested using a fuel cell measurement system (TAISIN Building System Co.). The working temperature of a single cell, as well as the temperature of the inlet and outlet for feeding gases of hydrogen and air, were maintained at 80 °C. The stoichiometry of the reactant in the anode and cathode was set at 1.5:2.0, with a relative humidity (RH) of 100%. The fuel cell performance was measured after being activated for 8 h. During the activation measurements, an exerted potential of 0.6 V was maintained for the scan control. During the polarization curve measurements, the exerted potential dropped from 0.9 to 0.3 V at 0.05 V intervals. Both the polarization and activation for the minimum flow rates for the anode and cathode were 200 and 1000 mLmin<sup>-1</sup>, respectively.

Cyclic voltammograms (CVs) were adopted in this study to obtain the ECSA for each of the cathodes, which can be estimated by calculating the adsorption or desorption of hydrogen on the Pt surface. The measurements were performed using a three-electrode electrochemical setup in an electrochemical station (CH Instruments, Inc.). An Ag/AgCl electrode (immersed in saturated KCl in advance) was used as the reference electrode, 1-cm<sup>2</sup> platinum plate was used as the counter electrode, 2-cm<sup>2</sup> sample (the ink sprayed on the carbon paper) was used as the working electrode, and 0.5 M H<sub>2</sub>SO<sub>4</sub> was used as the supporting electrolyte. Moreover, to ensure that the testing environment was not influenced by air, which contained O<sub>2</sub>, N<sub>2</sub> was aerated into the system. The voltage sweep was controlled from -0.241 V to 0.9 V with a scan rate of 50 mVs<sup>-1</sup>, and the number of sweep cycles was 100.

Electrochemical impedance spectroscopy (EIS) was performed on the same measurement system used for performance testing with identical working conditions. A Nyquist plot was established within a frequency range of 0.1 Hz to 20 kHz at three different current densities (200 mAcm<sup>-2</sup>, 450 mAcm<sup>-2</sup>, and 800 mAcm<sup>-2</sup>) with the disturbance current set at 10% of the operating current. In the Nyquist plot, the x-axis represents the actual impedance and the y-axis represents the imaginary impedance. The impedance arcs of all the samples under identical working conditions were fitted according to the equivalent circuit afforded by the Z-View software.

### 3. Results and Discussions

#### 3.1. Physical measurements

Fig. 2 shows SEM images of the CNTs and VGCFs at different weight percentages and the images of the CFs; the carbon materials can be easily observed in the red circles. As the CFs were significantly larger than the other carbon materials, it was not necessary to observe their distribution on the surface of the CCLs. In Fig. 2 (b1), (b2), and (b3), CNTs were not observed to exist in the CCLs until 3 wt%, and agglomeration occurred when 6 wt% CNT was added. Similarly, the VGCFs exhibited the same phenomenon as the CNTs; however, no agglomeration occurred in the 6 wt% VGCFs, which is shown as Fig. 2 (c3).

Table 2 suggests that all the electronic resistances of the CCLs decreased after adding the carbon materials with increasing magnitude as their weight percentage increased. The extent of decrease was the largest for the CFs, followed by that for VGCFs. Based on the fundamental properties of CNTs and VGCFs shown in Table 1, CNTs are smaller than VGCFs. Therefore, the number of added CNTs was much greater than that of the

VGCFs under identical added weights. In this situation, the continuity of electricity conduction for the CNTs was better than that for the VGCFs, although the length of VGCFs is longer than that of the CNTs. Schematic diagrams of these CCLs are shown in Fig. 3.

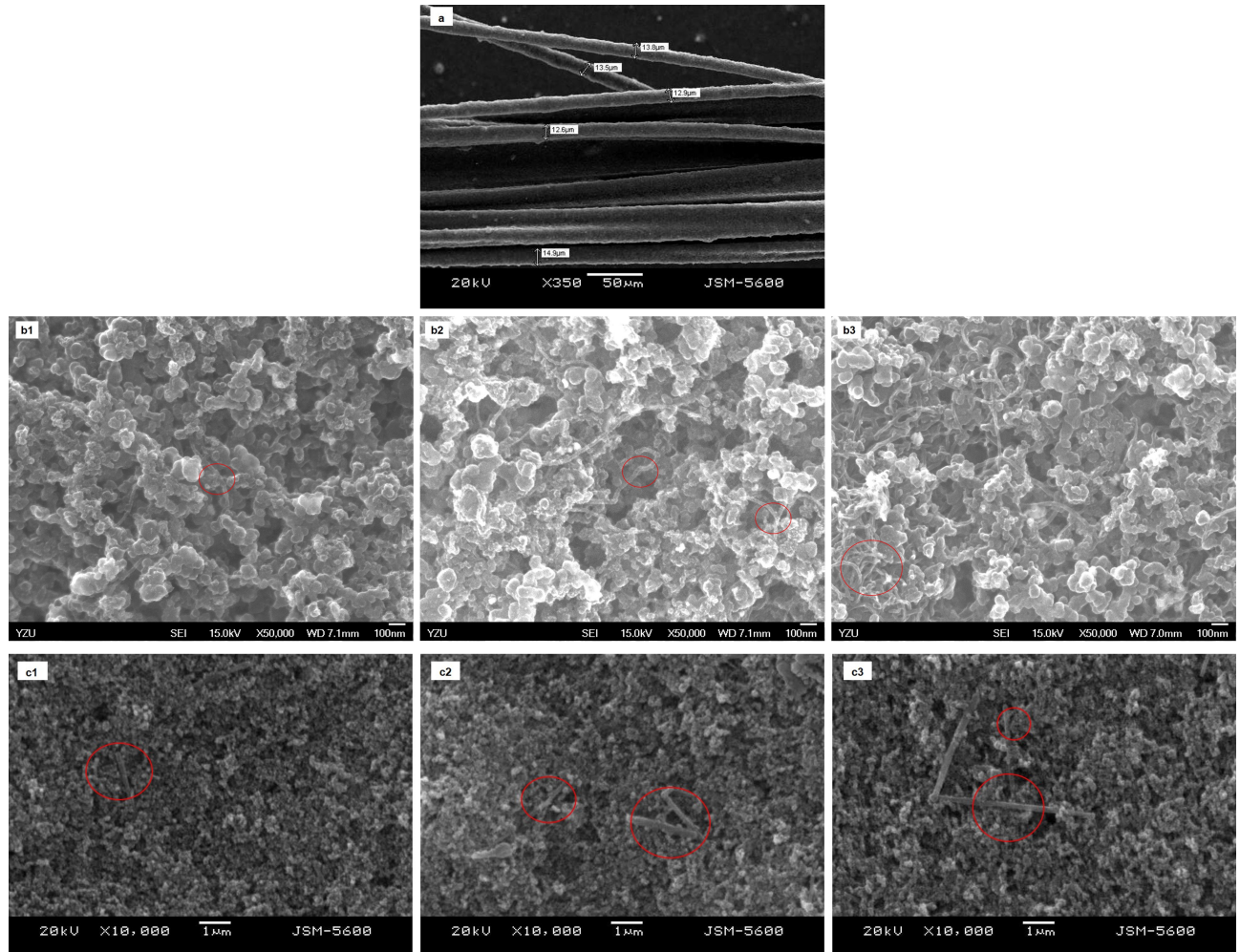


Fig. 2 (a) SEM image of the carbon fibers in CCL. SEM images of CNT additions at (b1) 1 wt%, (b2) 3 wt%, and (b3) 6 wt%, and of VGCF additions at (c1) 1 wt%, (c2) 3 wt%, and (c3) 6 wt% with respect to the weight of the Pt/C and Nafion®.

Table 2 Summary of electronic resistance of each electrode.

Sample	0 wt%	1 wt%	3 wt%	6 wt%
CFs	46.60	31.40	13.90	9.26
CNTs (MWCNTs)	46.60	30.75	24.60	19.57
VGCFs	46.60	39.00	38.60	35.15
Unit of electronic resistance: Ohm, Ω				

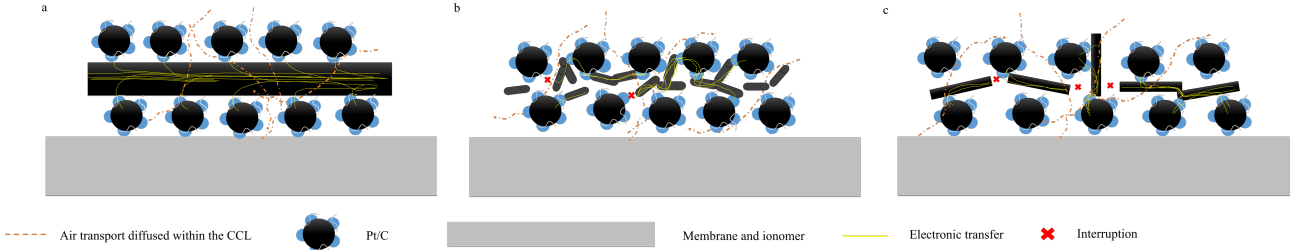


Fig. 3 Schematic of electronic transfer in MEAs within different carbon materials: (a) CFs added in CCLs, (b) CNTs added in CCLs, and (c) VGCFs added in CCLs

### 3.2. Electrochemical measurements

Fig. 4 shows the difference in the CV curves between the pristine and three carbon materials, i.e., CFs, CNTs, and VGCFs. The ECSA of each CCL was determined from the area of the hydrogen desorption peak in the CV curves. Apart from the CFs, the carbon materials had the tendency to increase proton accessibility, with the effect being greater as their weight percentage increased. For 3 wt%, both the CNTs and the VGCFs showed a 12% increase compared to the pristine. Significant growth was observed for the 6 wt% VGCFs; however, the CNTs at the same specific weight maintained a similar rate of increasing growth. For 6 wt%, the VGCFs increased by 35% compared to the pristine, while the CNTs only increased by 18%. It seemed that having extra space made the ECSA continually increase if the content of carbon materials was increased, but inks of higher concentration could not be sprayed out of the nozzle used.

Electrochemical impedance spectrum (EIS) analysis was performed to clarify the inner resistance of the MEAs with optimal addition contents by analyzing their ohmic resistance ( $R_\Omega$ ) and charge transfer resistance ( $R_{ct}$ ). The equivalent circuit shown in Fig. 5 was used to display Nyquist plots consisting of the raw data and the fitted data obtained via Z-View software. Fig. 6 shows the fitted Nyquist plots of the four MEAs, including the pristine, CFs, CNTs, and VGCFs with 6 wt% at different current densities. According to Table 3, the  $R_{ct}$  of the pristine was much larger than that of the rest of the MEAs. Most of the  $R_\Omega$  values remained the same, i.e., approximately  $0.15 \text{ } \Omega\text{cm}^{-2}$ . The lowest  $R_{ct}$  value was obtained with 6 wt% CFs when compared to same proportion of CNTs and VGCFs. Although this effect was not consistent when the current density was  $200 \text{ mA cm}^{-2}$ , it corresponded to the result that the ECSA of CFs did not provide any contribution to enhance the proton accessibility. However, according to the previous four-point probe measurement, CFs, with the highest continuity of electronic transportation, made the electronic charge transfer smoother and faster than CNTs and VGCFs. Moreover, the  $R_{ct}$  value of the 6 wt% CNTs was smaller than that of 6 wt% VGCFs due to the same principle. Therefore, based on the results of both four-point probe measurements and CV measurements, the electronic transfer resistance was the most crucial factor for  $R_{ct}$  in this study.

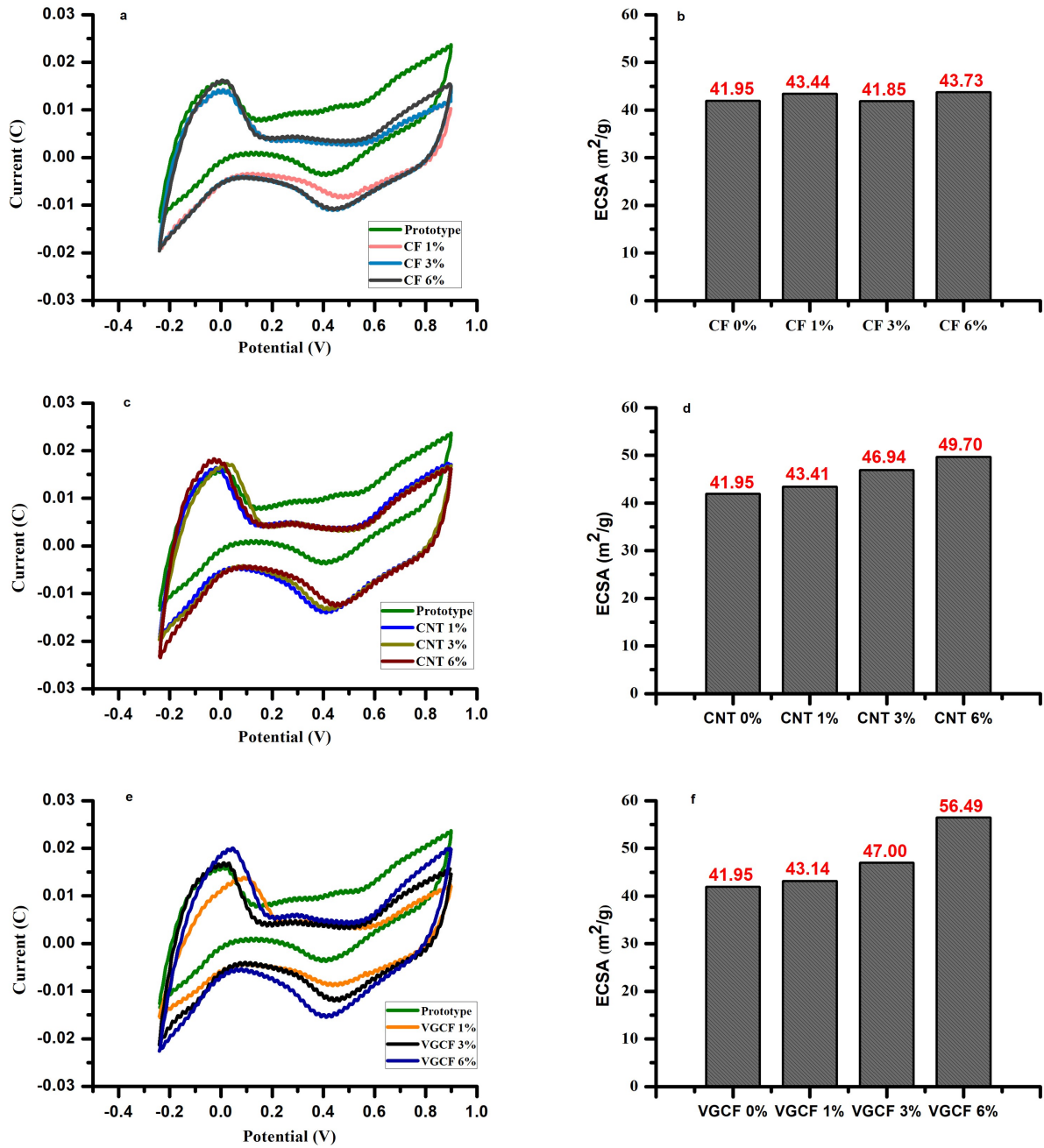


Fig. 4 Comparison of the CVs obtained for the three carbon materials with different specific weights and the pristine electrode: (a) CV curves of CFs, (b) histograms of ECSAs of CFs; (c) CV curves of CNTs, (d) histograms of ECSAs of CNTs; (e) CV curves of VGCFs, (f) histograms of ECSAs of VGCFs.

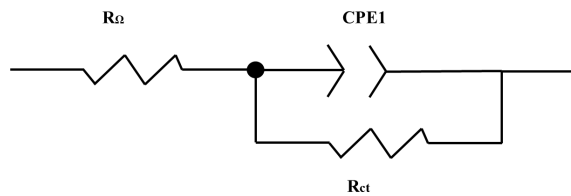


Fig. 5 EIS equivalent circuit

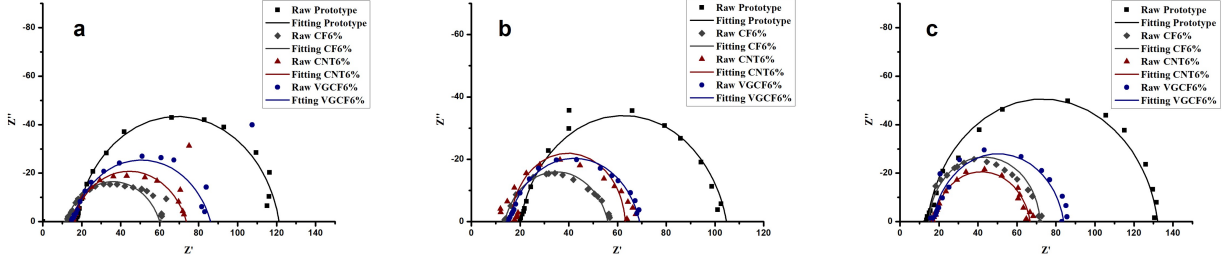


Fig. 6 EIS at (a) 200, (b) 450, and (c) 800  $\text{mAcm}^{-2}$  of the four MEAs including raw data, as denoted by dots, and fitted data, as denoted by curves.

Table 3 Ohmic resistance ( $R_\Omega$ ) and charge transfer resistance ( $R_{ct}$ ) of the four MEAs at different current densities.

Resistance of MEAs ( $\Omega\text{cm}^{-2}$ )	200 $\text{mAcm}^{-2}$		450 $\text{mAcm}^{-2}$		800 $\text{mAcm}^{-2}$	
	$R_\Omega$	$R_{ct}$	$R_\Omega$	$R_{ct}$	$R_\Omega$	$R_{ct}$
Pristine	0.14	1.04	0.20	0.64	0.17	0.86
CFs	0.15	0.41	0.14	0.28	0.16	0.43
CNTs (MWCNTs)	0.17	0.33	0.16	0.31	0.15	0.43
VGCFs	0.17	0.50	0.16	0.38	0.15	0.56

### 3.3. PEMFC Performances

Fig. 7 suggests that a higher power density was obtained by adding the CFs into the CCLs, which gradually increased with increasing CF weight percentage. Compared with the 1 wt% CFs electrodes yielding a maximum power density of the  $270 \text{ mWcm}^{-2}$ , the pristine showed only  $230 \text{ mWcm}^{-2}$ . As the weight percentage of the CFs increased, the power density of the 6 wt% sample increased considerably to  $450 \text{ mWcm}^{-2}$ , but reverse growth occurred after exceeding 6 wt%, i.e., when 12 and 15 wt% CF samples were used, the power density obtained was  $329$  and  $308 \text{ mWcm}^{-2}$ , respectively. Moreover, adding CNTs and VGCFs significantly increased the power density to  $397$  and  $354 \text{ mWcm}^{-2}$ , respectively. Herein, at least  $\sim 345 \text{ mWcm}^{-2}$  was obtained when these two materials were added, although the difference in the distinct weight percentage was marginal. Compared with the power density of the pristine, the 6 wt% CFs increased by 96%; in addition, power densities of the CCLs with 6 wt% CNTs and CCLs with 6 wt% VGCFs increased by 73% and 54%, respectively.

As stated previously, the concentration of ink was sufficiently high to spray out from the nozzle if more than 6 wt% of the CNTs and VGCFs was added; therefore, the optimal additions for the CNTs and VGCFs was approximately 6 wt%. Finally, by integrating all the optimal added proportions for each electrode, the differences between each other in distinct regions of the fuel cell polarization were examined and analyzed. In active polarization, the performances of VGCFs and CFs were the best and worst, respectively. This result was consistent with the effect of ECSA, in which adding CFs was not beneficial for increasing the ECSA. In the ohmic polarization, the slopes of the CFs and VGCFs were the smallest and the largest, respectively. In terms of the contribution of VGCF, it provided a catalyst layer with a higher porosity and slightly reduced the electronic resistance. In contrast, although the CF electrode did not influence the ECSA, it contributed to a lower total catalyst layer resistance, which is the sum of ionic and electronic resistances in the CCLs, owing to the tremendous decrease in electronic resistance. This result also corresponded to the measurement of both the four-point probes and EIS analysis.

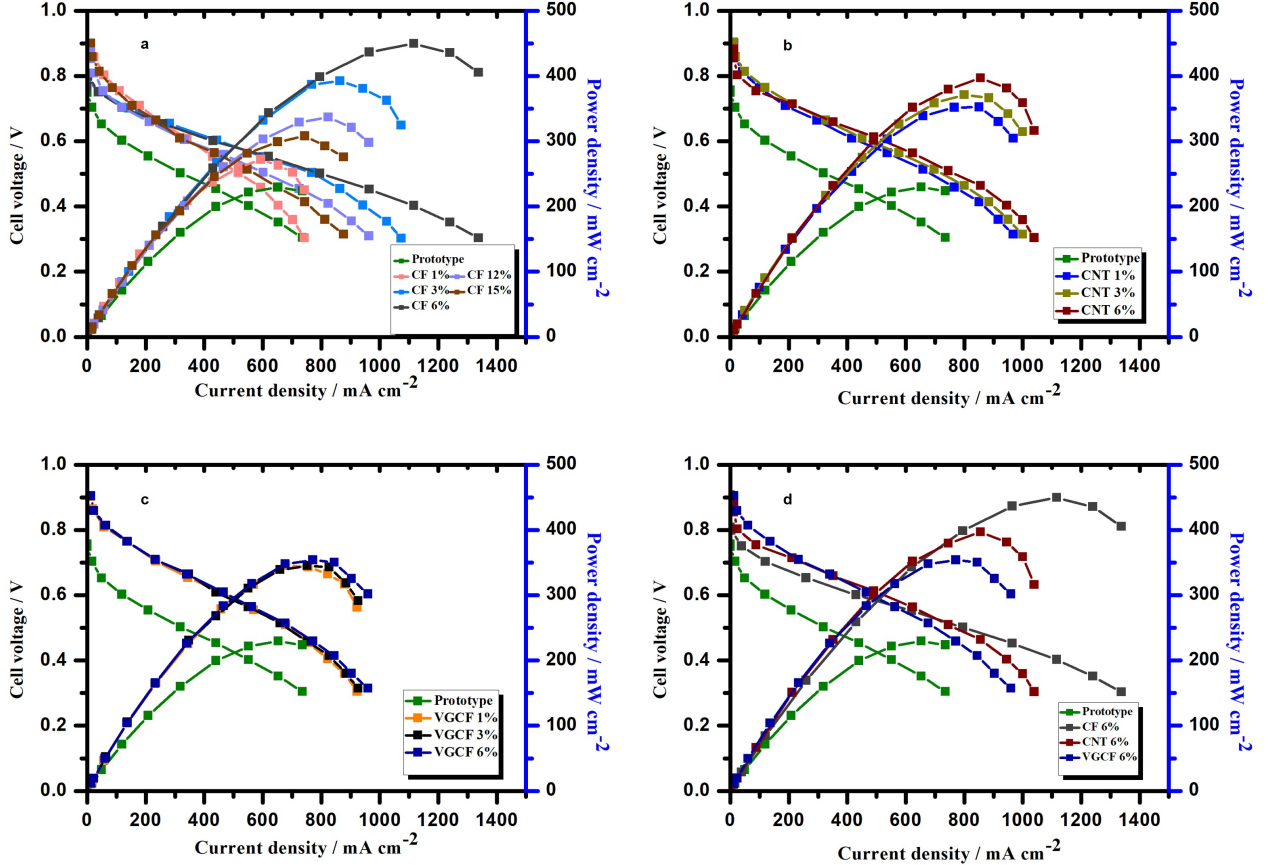


Fig. 7 Comparison of fuel cell performance obtained for the three carbon materials with the pristine electrode. (a) I-V curve of CFs, (b) VGCFs, and (c) CNTs. (d) Optimal I-V curves of CFs, VGCFs, and CNTs. Fuel cell testing was performed at 80 °C with humidified H<sub>2</sub> and air gas. Performances are shown as a figure incorporated cell voltage vs. current density with power density vs. current density.

#### 4. Conclusions

Three additives were employed to fabricate the CCLs in this study. Based on the exact same Pt/C catalyst and diagnostic methods, including SEM, four-point probing measurement system, CV, EIS, and polarization curves, the differences in the effects of CF, CNT, and VGCF additions to CCLs were studied. The CV results suggested that an MEA with CFs did not negatively interfere with the ability of Pt for hydrogen desorption, but one with CNTs and VGCFs strengthened the ability. This was because CNTs and VGCFs effectively increased the porosity of the catalyst layer, which resulted in an increase in the ECSA. Furthermore, the electronic resistance of the catalyst layer was significantly reduced by adding CFs, CNTs, and VGCFs to the CCLs. This effect was verified by four-point probe and EIS measurements. Hence, the total catalyst layer resistance was reduced by the abovementioned effects. Compared to the pristine (only Pt/C), all three materials significantly increased the performance of the fuel cell. However, longer carbon materials exhibited superior performance, and this result is based on the continuity of electronic transport. An optimal CCL performance was achieved with approximatively 6 wt% of the additives. VGCFs improved the performance by notably

increasing the porosity of the catalyst layer, but they did not effectively enhance the electronic transport. In contrast, CFs provided smooth electronic paths to accelerate electronic transport. As a result, the increase in electron paths to reduce the electronic resistance was the most prominent factor for improving the performance of the fuel cells in this study.

## 5. Acknowledgements

The authors would like to thank Ministry of Science and Technology (MOST), Taiwan for the financial support through grant MOST-109-2622-E-155-013.

## 6. References

- [1] Ogungbemi E., Wilberforce T., Ijaodola O., Thompson J., Olabi A, Selection of proton exchange membrane fuel cell for transportation, International Journal of Hydrogen Energy, 2020,  
<https://doi.org/10.1016/j.ijhydene.2020.06.147>
- [2] Ren X., Lv Q., Liu L., Liu B., Wang Y., Liu A., Wu G., Current progress of Pt and Pt-based electrocatalysts used for fuel cells, Sustainable Energy & Fuels, 2020, 4(1), 15-30,  
<https://doi.org/10.1039/C9SE00460B>
- [3] Seo D., Kim M., Yang S., Choi W., Choi H., Choi S., Lee M., Yoon Y., Seo M., Kim H., Jung C., Kim T, Nitrogen-doped carbon supported platinum catalyst via direct soft nitriding for high-performance polymer electrolyte membrane fuel cell, International Journal of Hydrogen Energy, 2018, 43(37), 17873-17879,  
<https://doi.org/10.1016/j.ijhydene.2018.07.173>
- [4] Haj Ibrahim S., Wejrzanowski T., Sobczak P., Cwieka K., Lysik A., Skibinski J., Oliver G., Insight into cathode microstructure effect on the performance of molten carbonate fuel cell, Journal of Power Sources, 2021, 491, 229562, <https://doi.org/10.1016/j.jpowsour.2021.229562>
- [5] Zhang R., Min T., Liu Y., Chen L., Tao W., Pore-scale study of effects of different Pt loading reduction schemes on reactive transport processes in catalyst layers of proton exchange membrane fuel cells, International Journal of Hydrogen Energy, 2021, 46(38), 20037-20053,  
<https://doi.org/10.1016/j.ijhydene.2021.03.124>
- [6] Vuppala R., Chaedir B., Jiang L., Chen L., Aziz M., Sasmito A., Optimization of Membrane Electrode Assembly of PEM Fuel Cell by Response Surface Method, Molecules, 2019, 24(17), 3097,  
<https://doi.org/10.3390/molecules24173097>
- [7] Xing L., Shi W., Su H., Xu Q., Das P., Mao B., Scott K., Membrane electrode assemblies for PEM fuel cells: A review of functional graded design and optimization, Energy, 2019, 177, 445-464,  
<https://doi.org/10.1016/j.energy.2019.04.084>
- [8] Berlinger S., Garg S., Weber A, Multicomponent, multiphase interactions in fuel-cell inks, Current Opinion in Electrochemistry, 2021, 29, 100744, <https://doi.org/10.1016/j.coelec.2021.100744>

- [9] Liu G., Ding X., Zhou H., Chen M., Wang M., Zhao Z., Yin Z., Wang X., Structure optimization of cathode microporous layer for direct methanol fuel cells, *Applied Energy*, 2015, 147, 396-401, <https://doi.org/10.1016/j.apenergy.2015.03.021>
- [10] Talukdar K., Delgado S., Lagarteira T., Gazdzicki P., Friedrich K., Minimizing mass-transport loss in proton exchange membrane fuel cell by freeze-drying of cathode catalyst layers, *Journal of Power Sources*, 2019, 427, 309-317, <https://doi.org/10.1016/j.jpowsour.2019.04.094>
- [11] Deng X., Zhang J., Fan Z., Tan W., Yang G., Wang W., Zhou W., Shao Z., Understanding and Engineering of Multiphase Transport Processes in Membrane Electrode Assembly of Proton-Exchange Membrane Fuel Cells with a Focus on the Cathode Catalyst Layer: A Review, *Energy Fuels* 2020, 34(8), 9175-9188, <https://doi.org/10.1021/acs.energyfuels.0c02101>
- [12] Hou J., Yang M., Ke C., Wei G., Priest C., Qiao Z., Wu G., Zhang J., Platinum-group-metal catalysts for proton exchange membrane fuel cells: From catalyst design to electrode structure optimization, *EnergyChem*, 2020, 2(1), 100023, <https://doi.org/10.1016/j.enchem.2019.100023>
- [13] Li B., Xie M., Ji H., Chu T., Yang D., Ming P., Zhang C., Optimization of cathode microporous layer materials for proton exchange membrane fuel cell, *International Journal of Hydrogen Energy*, 2021, 46(27), 14674-14686, <https://doi.org/10.1016/j.ijhydene.2021.01.169>
- [14] da Silva G., Fernandes M., Ticianelli E., Activity and Stability of Pt/IrO<sub>2</sub> Bifunctional Materials as Catalysts for the Oxygen Evolution/Reduction Reactions, *ACS Catalysis*, 2018, 8(3), 2081-2092, <https://doi.org/10.1021/acscatal.7b03429>
- [15] Osgood H., Devaguptapu S., Xu H., Cho J., Wu G., Transition metal (Fe, Co, Ni, and Mn) oxides for oxygen reduction and evolution bifunctional catalysts in alkaline media, *Nano Today* 2016, 11(5), 601-625, <https://doi.org/10.1016/j.nantod.2016.09.001>
- [16] Zhang X., Li H., Yang J., Lei Y., Wang C., Wang J., Tang Y., Mao Z., Recent advances in Pt-based electrocatalysts for PEMFCs, *RSC Advances*, 2021, 11(22), 13316-13328, <https://doi.org/10.1039/D0RA05468B>
- [17] Samad S., Loh K., Wong W., Lee T., Sunarso J., Chong S., Wan Daud W., Carbon and non-carbon support materials for platinum-based catalysts in fuel cells, *International Journal of Hydrogen Energy*, 2018, 43(16) 7823-7854, <https://doi.org/10.1016/j.ijhydene.2018.02.154>
- [18] Xiao Y., Wang W., Li T., Mao Y., Liu C., Onion-like Core-shell Ni@C supported on carbon nanotubes decorated with low Pt as a superior electrocatalyst for hydrogen evolution reaction, *Electrochimica Acta*, 2021, 386, 138406, <https://doi.org/10.1016/j.electacta.2021.138406>
- [19] Rathinavel S., Priyadarshini K., Panda D., A review on carbon nanotube: An overview of synthesis, properties, functionalization, characterization, and the application, *Materials Science & Engineering B*, 2021, 268, 115095, <https://doi.org/10.1016/j.mseb.2021.115095>
- [20] Hou S., Chi B., Liu G., Ren J., Song H., Liao S., Enhanced performance of proton exchange membrane fuel cell by introducing nitrogen-doped CNTs in both catalyst layer and gas diffusion layer, *Electrochimica Acta*, 2017, 253, 142-150, <https://doi.org/10.1016/j.electacta.2017.08.160>
- [21] Haque M., Sulon A., Shyuan L., Majlan E., Husaini T., Rosli R., Synthesis of polymer/MWCNT nanocomposite catalyst supporting materials for high-temperature PEM fuel cells, *International Journal of*

Hydrogen Energy, 2021, 46(5), 4339-4353, <https://doi.org/10.1016/j.ijhydene.2020.10.200>

[22] Mabena L., Makgopa K., Tanko-Djoubi A., Modibane K., Hato M., Nanostructured Carbon-Based Materials for Fuel Cell Applications, Carbon Related Materials, 2021, 357-390, [https://doi.org/10.1007/978-981-15-7610-2\\_15](https://doi.org/10.1007/978-981-15-7610-2_15)

[23] Zhao J., Tu Z., Chan S., Carbon corrosion mechanism and mitigation strategies in a proton exchange membrane fuel cell (PEMFC): A review, Journal of Power Sources, 2021, 488, 229434, <https://doi.org/10.1016/j.jpowsour.2020.229434>

[24] Esteves L., Oliveira H., Passos F., Carbon nanotubes as catalyst support in chemical vapor deposition reaction: A review, Journal of Industrial and Engineering Chemistry, 2018, 65, 1-12, <https://doi.org/10.1016/j.jiec.2018.04.012>

[25] Chernyak S., Suslova E., Egorov A., Lu L., Savilov S., Lunin V., New hybrid CNT–alumina supports for Co-based Fischer–Tropsch catalysts, Fuel Processing Technology, 2015, 140, 267-275, <https://doi.org/10.1016/j.fuproc.2015.09.012>

[26] Sun M., Xie Z., Li Z., Deng X., Huang Q., Electrospun iron and nitrogen co-containing porous carbon nanofibers as high-efficiency electrocatalysts for oxygen reduction reaction, International Journal of Hydrogen Energy, 2019, 44(45), 24617-24627, <https://doi.org/10.1016/j.ijhydene.2019.07.182>

[27] Wei Z., Wang J., Mao S., Su D., Jin H., Wang Y., Xu F., Li H., Wang Y., In Situ-Generated  $\text{Co}^0$ - $\text{Co}_3\text{O}_4$ /N-Doped Carbon Nanotubes Hybrids as Efficient and Chemoselective Catalysts for Hydrogenation of Nitroarenes, ACS Catalysis, 2015, 5(8), 4783-4789, <https://doi.org/10.1021/acscatal.5b00737>

[28] Singh K., Tetteh E., Lee H., Kang T., Yu J., Tailor-Made Pt Catalysts with Improved Oxygen Reduction Reaction Stability/Durability, ACS Catalysis, 2019, 9(9), 8622-8645, <https://doi.org/10.1021/acscatal.9b01420>

[29] Park S., Jung D., Kim S., Lim S., Peck D., Hong W., The effect of vapor-grown carbon fiber as an additive to the catalyst layer on the performance of a direct methanol fuel cell, Electrochimica Acta, 2009, 54(11), 3066-3072, <https://doi.org/10.1016/j.electacta.2008.11.066>

[30] Pillai A., Chandran A., Peethambharan S., MWCNT Ink with PEDOT: PSS as a multifunctional additive for energy efficient flexible heating applications, Applied Materials Today, 2021, 23, 100987, <https://doi.org/10.1016/j.apmt.2021.100987>

[31] Cheng X., Zhang J., Shi Z., Glass N., Zhang L., Song D., Liu Z., Wang H., Shen J., A review of PEM hydrogen fuel cell contamination: Impacts, mechanisms, and mitigation, Journal of Power Sources, 2007, 165 (2), 739-756, DOI:[10.1016/j.jpowsour.2006.12.012](https://doi.org/10.1016/j.jpowsour.2006.12.012)